1. Supplementary material

1.1. Experimental section

A high-sensitivity multichannel notch-filtered INFINITY spectrograph (Jobin-Yvon-Horiba SAS, Longjumeau, France) equipped with a Peltier cooled CCD matrix detector was used to record Raman spectra between ~150 and 2000 cm^{-1}, using 532 and 632 nm exciting lines (YAG and He-Ne lasers). Backscattering illumination and collection of the scattered light were made through an Olympus confocal microscope (long focus Olympus x10 and x50 objective, total magnification x100 and x500). Special attention was paid to the power of illumination used (0.1-2 mW). The data collection was carried out on small particle aggregates, in a procedure preferentially used for a dark material.

Synchrotron X-ray experiments were performed at room temperature at the 6-ID-D beamline at the Advanced Photon Source at Argonne National Laboratory, Argonne, IL. Details of the experiment and data treatment could be found in Kremenovic *et al.* (2011).

The X-ray line broadening was analyzed by the Breadth computer program (Balzar, 1992). The Breadth program calculates microstructural parameters according to the Warren–Averbach (WA) and simplified integral breadth (SIB) methods (Balzar, 1993; Klug & Alexander, 1974). The X-ray line broadening of the *hh*0 ($h = 1, \ldots, 5$) reflections was analyzed. Input data for the Breadth program, such as unit-cell parameters, peak positions (2θmax), FWHM (full-width half-maximum) and Lorenz/Gauss mixing components (η), were taken from the output of the FullProf program.

The role of the specimen and the crystallite statistics for an XRPD experiment (experiment involving intensity measurements) are very important. The number of crystallites that contribute to the diffraction spectrum is limited by their size, the volume of the specimen in the beam, and whether the specimen was moving during the measurements. There are a number of ways to increase this number for a given instrument. The easiest way is to reduce the crystallite size to dimensions around 1 μm, but this is not always possible. Therefore the specimen size could be the limiting factor in the experiment. However, we prepared nanopowders with an average grain size between few tens to a few hundreds of angstroms (Kremenovic *et al.*, 2011). In this way, we were able to conclude that our profile analyses were accurate and reliable. Moreover, the Debye rings on 2D XRPD pattern are very well defined and continuous, indicating good crystallite statistics, Figure s3.

1.2. Raman data processing

The Raman spectra of nanocrystalline materials are usually simulated by phenomenological phonon confinement model (PCM), in which several independent factors, like phonon confinement, strain, non–

homogeneity of the size distribution, defects and variations in phonon relaxation with crystallite size decreasing contribute to the position and linewidth of calculated Raman mode (Campbell *et al.*, 2001, Spanier *et al.*, 2001, Šćepanović *et al.*, 2007). Due to decrease of crystallite size, the phonons are confined and optical phonons over the entire Brillouin zone (BZ) contribute to the first-order Raman spectra. The Raman spectrum is obtained by integrating these contributions over the complete BZ, according to Richter *et al.* (Richter *et al.*, 1981) and Campbell and Fauchet (Campbell *et al.*, 2001), as:

$$I(\omega) \propto \int_{BZ} \mathrm{d}^3 q \frac{\left|C(0,\vec{q})\right|^2}{[\omega - \omega(q)]^2 + \left(\Gamma_0 / 2\right)^2}, \quad (1)$$

where $\omega(q)$ is the phonon dispersion curve, q - wave vector, Γ_0 - natural linewidth of the zone-centre optical phonon in the bulk (full width at half-maximum), and $C(0,q)$ is the Fourier coefficient of the phonon confinement function (Arora *et al.*, 2007; Richter *et al.*, 1981). For the Gaussian confinement this coefficient is given by

$$\left|C(0,q)\right|^2 \cong \exp(-q^2 L^2 / 8\beta), \quad (2)$$

with nanoparticle size diameter L, and adjustable confinement strength β, proposed to be $\beta=1$ by Richter (Richter *et al.*, 1981), and $\beta=2\pi^2$ by Campbell and Fauchet (Campbell and Fauchet, 2001). In case of column shape Fourier coefficient is taken as (Arora *et al.*, 2007; Cheng *et al.*, 2005, Mazza *et al.*, 2007):

$$\left|C(0,q_{1,}q_2)\right|^2 \cong \exp(-q^2 L_1^2 / 8\beta)\exp(-q^2 L_2^2 / 8\beta) \times \left|1 - erf[iq_2 L_2 / 4\sqrt{\beta}]\right|^2, \quad (3)$$

where L_1 and L_2 are the diameter and length of the cylinder structure. It is usually assumed that the length of such nanostructure is much larger than its diameter; therefore the terms containing L_2 may be neglected, as the confinement effect is mainly occurring along the diameter direction (Cheng *et al.*, 2005).

The BZ is assumed to be homogeneous and isotropic sphere, and the integration presented in Eq. (1) is performed in spherical coordinates over n dispersion curves $\omega(q)$, depending on mode degeneration n (Spanier *et al.*, 2001; Šćepanović *et al.*, 2007). The Raman peaks have been also shifted by the value of $\Delta\omega$ due to the strain effect, depending on relative variation of unit cell dimensions (Spanier *et al.*, 2001).

The anatase and rutile E_g modes are modeled by PCM in order to estimate the dimension of anatase nanoparticles, as well as the diameter of rutile nanorods. The Raman modes of anatase nanoparticles are fitted by 3D PCM (Eqs. (1) and (2)), and modes of rutle nanorods by 2D PCM (Eqs. (1) and (3)). The

influence of the dimensionality of phonon confinement on the position and linewidth of Raman mode is manifested in less shifted and less broadened modes in the spectra of materials confined to one dimension (such as nanorods) in comparison to objects such as nanoparticles, confined in all dimensions (Arora *et al.*, 2007).

In spectra of samples without Fe content (Fig. 1) and with 1.05 %Fe (Fig. s2) the most intensive anatase Raman mode E_g is calculated by usually used 3D PCM described above (Campbell and Fauchet, 1986; Šćepanović *et al.*, 2007; Spanier *et al.*, 2001). The phonon dispersion curves have been taken in usual cosine form to fit the theoretical phonon-band structure of anatase, as $\omega_i(q) = A + B_i\ (1 - \cos(\pi q)$, with parameters chosen to correspond to 3 directions of high symmetry in anatase BZ (Mikami *et al.*, 2002; Šćepanović *et al.*, 2007). The integration defined by Eqs.(1) and (2) is thus performed over the whole BZ, with mode degeneracy and symmetry of directions taken into account.

The diameters of cylindrical nanoparticles of rutile have been estimated from the 2D PCM (Mazza *et al.*, 2007; Cheng *et al.*, 2005) of the rutile E_g mode from the Raman spectra of samples with 0, 0.22, and 0.47% (Figs. s1a and s1b). Corresponding phonon dispersions in PCM have been taken in cosine form usually used in literature (Mazza *et al.*, 2007; Swamy 2008). The influence of rutile lattice strain to Raman modes has been included in PCM through the form of average strain, i.e. relative variation of unit cell volume ($\Delta V/V_0$) calculated from XRPD data for lattice parameters (Kremenovic *et al.*, 2011).

References:

Arora, A. K., Rajalakshmi, M., Ravindran, T. R. Sivasubramanian, V. (2007) *J. Raman Spectroscopy* **38,** 604–617.

Campbell, I. I., Fauchet, P. M. (1986) *Solid State Commun.* **58(10)**, 739-741.

Cheng, C. L., Chen, Y. F., Chen, R. S., Huang Y. S. (2005) *Appl. Phys. Lett.* **86**, 103104.

Kremenović, A., Antić, B., Blanuša, J., Čomor, M., Colomban, P., Mazerolles, L., Bozin, E.S. (2011) *Journal of Physical Chemistry C* **115**, 4395-4403.

Mazza, T., Barborini, E., Piseri,P., Milani, P., Cattaneo, D., Li Bassi, A., Bottani, C. E., Ducati, C. (2007) *Phys. Rev. B* **75**, 045416(1-5).

Mikami, M., Nakamura, S., Kitao, O., Arakawa, H. (2002) *Phys. Rev. B* **66**, 155213(1-6).

Richter H., Wang, Z.P., Ley, L. (1981) *Solid State Commun.* **39**, 625–629.

Spanier, J. E., Robinson, R. D., Zhang, F., Chan, S.-W., Herman, I.P. (2001) *Phys. Rev. B* **64**, 245407(1-8).

Šćepanović, M., Grujić-Brojčin, M., Dohčević-Mitrović, Z., Popović, Z. V. (2007) *Appl. Phys.A* **86**, 365–371.

Swamy, V. (2008) *Phys. Rev. B* **77**, 195414(1-4).

Table s1. The Raman shift and linewidth (in parentheses) of anatase and rutile modes in the spectra of titania samples with 0, 0.22, 0.47 and 1.05 at% Fe. The nanoparticle/nanorod diameters, estimated from PCM, are also listed.

	Anatase					Rutile			
at% Fe	Particle size (nm)	Raman shift (linewidth) (cm^{-1})				Particle size (nm)	Raman shift (linewidth) (cm^{-1})		
		E_g (PCM)	B_{1g}	$A_{1g}+B_{1g}$	E_g		2^{nd} ord.	E_g (PCM)	A_{1g}
0	10.0	145 (16)	399 (35)	520 (28)	638 (47)	7.0	240 (88)	445 (40)	610 (43)
0.22	-	-	-	-	-	4.0	248 (62)	443 (52)	611 (46)
0.47	-	-		-	-	3.5	248 (68)	442 (54)	610 (40)
1.05	8.0	146.8 (19)	397 (30)	520 (35)	635 (40)	-	-	-	-

Table s2. The Raman shift brookite modes, located in the spectra of titania samples with 0, 0.22, 0.47 and 1.05 % Fe, assigned from the Tompsett *et al.* (1994).

at%	Brookite modes, Raman shift (cm^{-1})													
% Fe	B_{3g}	A_{1g}	B_{3g}	B_{1g}	A_{1g}	B_{3g}	B_{1g}	B_{3g}	A_{1g}	B_{1g}	A_{1g}	B_{3g}	B_{2g}	A_{1g}
0	122	150	-	-	240	280	320	360	-	-	-	550	-	640
0.22	-	~150	-	210	-	287	320	366	-	-	-	558	580	638
0.47	-	~160	-	215	-	-	320	366	-	-	-	540	580	640
1.05	120	160	175	215	-	-	-		412	460	505	-	-	640

Table s3. The rutile microstructure size-strain parameters of samples with 0, 0.22, 0.47 and 1.05 at% Fe.

at% Fe	0	0.22	0.47	1.05
Warren-Averbach method				
a_3' (Å)	1.8	1.8	2.1	2.1
$\langle D \rangle_S$ (Å)	33±5	21±3	26±3	26±4
$\langle D \rangle_V$ (Å)	37±2	34±2	39±3	39±3
$\langle \varepsilon^2 \rangle^{1/2}_{\langle D \rangle S/2} \cdot 10^2$	0.5 ± 0.1	0.41 ± 0.01	0.32 ± 0.01	0.31 ± 0.01
$\langle \varepsilon^2 \rangle^{1/2}_{\langle D \rangle V/2} \cdot 10^2$	0.5 ± 0.1	0.34 ± 0.01	0.27 ± 0.01	0.27 ± 0.01
$\langle \varepsilon^2 \rangle^{1/2} a_3' \cdot 10^2$	1.5 ± 0.3	0.90 ± 0.02	0.71 ± 0.02	0.70 ± 0.01
$\langle \varepsilon^2 \rangle^{1/2}_{Gauss} \cdot 10^2$	0.6 ± 0.1	0.19 ± 0.01	0.15 ± 0.01	0.15 ± 0.01
Simplified integral breadth method				
$\langle D \rangle_{LL}$ (Å)	41	35	40	40
$\langle D \rangle_{LG}$ (Å)	37	34	39	39
$\langle D \rangle_{GG}$ (Å)	36	34	39	39
$\langle \varepsilon^2 \rangle^{1/2}_{LL} \cdot 10^2$	0.33	0.14	0.10	0.10
$\langle \varepsilon^2 \rangle^{1/2}_{LG} \cdot 10^2$	0.51	0.40	0.31	0.31
$\langle \varepsilon^2 \rangle^{1/2}_{GG} \cdot 10^2$	0.67	0.55	0.43	0.43

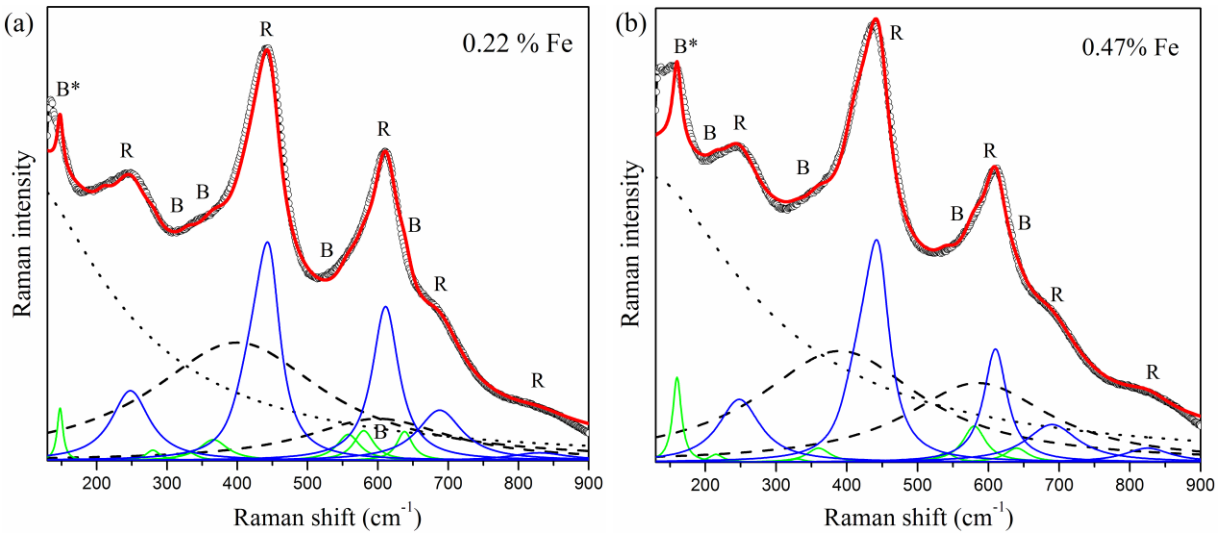

Figure s1. The experimental Raman spectrum of the samples with 0.22 (a) and 0.47 at%Fe (b), both fitted by the sum of the most intense rutile E_g(R) mode obtained by PCM, and other rutile (R) and brookite (B) modes fitted by the Lorentzians (open symbols – experimental spectrum, continuous lines – calculated modes for rutile and brookite modes, denoted by corresponding letters, as well as overall calculated profile, dotted line – bosonlike contribution and dashed lines – amorphous titania features).

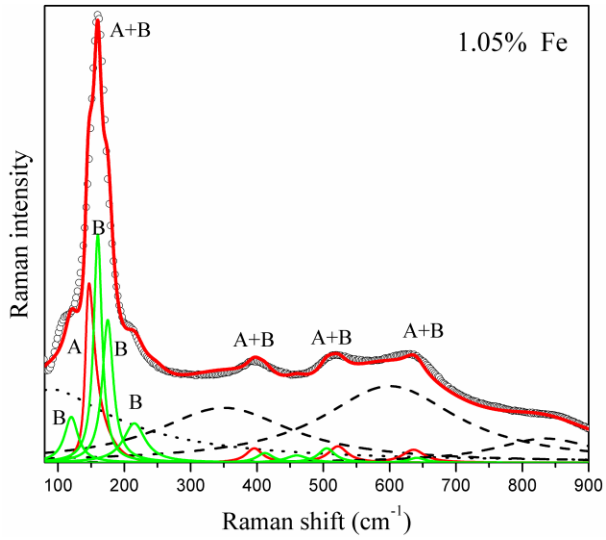

Figure s2. The experimental Raman spectrum of the sample with 1.05 at% Fe, calculated by the sum of the most intense anatase E_g(A) mode obtained by PCM, and anatase (A) and brookite (B) modes fitted by the Lorentzians (open symbols – experimental spectrum, continuous lines – calculated modes for anatase and brookite modes, denoted by corresponding letters, as well as overall calculated profile, dotted line – bosonlike contribution and dashed lines – amorphous titania features).

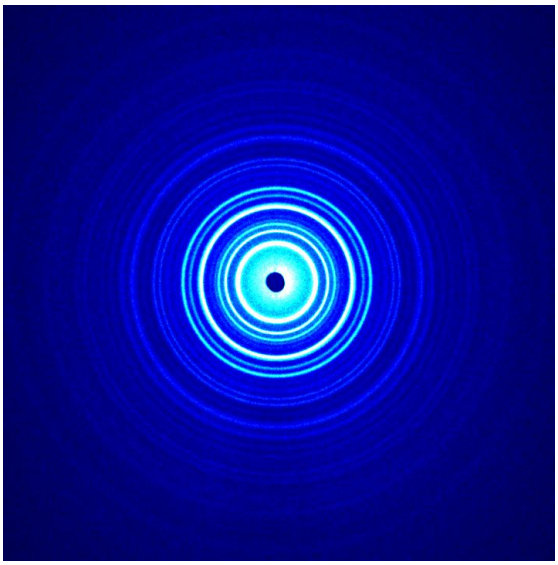

Figure s3. 2D diffraction pattern obtained at 6-ID-D at APS for pure TiO_2. Notice that Debye rings are very well defined and continuous, providing good crystallite statistics.